

Uranium Doping and Thermal Neutron Irradiation Flux Pinning Effects in MgB₂

T. Silver^{1*}, J. Horvat¹, M. Reinhard², Y. Pei³, S. Keshavarzi¹, P. Munroe⁴, and S.X. Dou¹

¹*Institute for Superconducting and Electronic Materials, University of Wollongong, Northfields Avenue, Wollongong 2522, Australia*

²*Safety and Radiation Science, Australian Nuclear Science and Technology Organisation (ANSTO), Lucas Heights 2234, Australia*

³*Centre for Electron Microscope Analysis, Tienjun University, TienJun, PRC*

⁴*Electron Microscopy Unit, University of New South Wales, Sydney 2052, Australia*

ABSTRACT

The U/n method is a well-established means of improving flux pinning and critical current performance in cuprate superconductors. The method involves the doping of the superconductor with ²³⁵U followed by irradiation with thermal neutrons to promote fission. The resultant columnar damage tracks produced by the energetic fission products pin flux vortices and improve critical current performance in magnetic fields. No such improvement could be observed when the U/n method was applied to MgB₂ superconductor. No fission tracks could be observed in TEM, even for samples that were irradiated at the highest fluence. Gamma-ray spectroscopy indicated that fission had occurred in the expected way.

PACS numbers: 74.70.Ad, 74.25.Qt, 61.80.Hg

Keywords: MgB₂; U/n method; Uranium doping; Flux pinning

1. INTRODUCTION

Since its superconducting properties were first discovered in 2001 [1, 2], MgB₂ has been found to share characteristics with both conventional low temperature superconductors (LTS) and with cuprate high temperature superconductors (HTS). Its critical temperature T_c is nearly 40K, unusually high for a non-cuprate material. MgB₂ behaves like a conventional type-II superconductor in relation to the isotope effect, the T-dependence of the upper critical field, and resistivity R(T) measurements, but more like the HTS superconductors in the temperature dependence λ(T) of the penetration depth and the behaviour of the Hall coefficient near T_c [3]. Although MgB₂ films have attained critical currents above 10⁶ A/cm² at 4.2K in low magnetic fields [4], MgB₂ [3] and the HTS cuprates [5] share a rapidly decreasing J_c(H) performance as magnetic fields increase compared to LTS superconductors such as Nb₃Sn and Nb-Ti. In HTS materials the field performance is related to both weak links between grains and poor flux pinning behaviour. The former consideration does not apply to MgB₂, as transport measurements of J_c and measurements calculated from magnetic hysteresis loops yield very similar results, indicating that the flow of super-current is not hindered by grain boundaries [6, 7]. The flux creep in MgB₂ is much weaker than in average HTS [8, 9], indicating stronger vortex pinning. However, this pinning should still be improved to offset the effect of the low H_{c2} of MgB₂ (about 18T) [10] on the field dependence of J_c.

* Corresponding author: Tania M. Silver, Institute for Superconducting and Electronic Materials, Faculty of Engineering, University of Wollongong, Northfields Ave., Wollongong, NSW 2522, Australia; telephone: (02) 4221 5766; fax: (02) 4221 5731; e-mail: tsilver@uow.edu.au.

Superconductivity above H_{c1} in any type-II material depends on flux pinning in regions where the superconducting order parameter is reduced, either by intrinsic features of the crystal structure or by point or extended defects. Otherwise the flux vortices would move individually or collectively due to Lorentz forces when a uniform current is applied, resulting in local superconducting phase slip and a non-zero electrical resistance [11]. There is a long history of attempts, often successful, to improve $J_c(H)$ performance by creating strong pinning centres in HTS superconductors, by means such as the introduction of precipitates and the use of a variety of irradiation techniques employing neutrons, heavy ions, electrons and protons [5]. Some methods of introducing pinning centres have also been successful with MgB_2 , including oxygen alloying in thin films [4] and the addition of nano-scale particles of SiC [12] and Si [13], as well as irradiation with protons [14]. Attempts have also been made using irradiation with heavy ions [15, 16] and neutrons [17, 18], although reported effects from these two methods have been small to date.

One irradiation method that has not yet been reported for MgB_2 is the U/n [19, 20] method, although it has been highly successful in improving flux pinning in HTS. The U/n method differs from straightforward irradiation with thermal neutrons, in that the material is first doped with compounds containing ^{235}U . When irradiation takes place the ^{235}U atoms absorb thermal neutrons and fission. The two fission products recoil in opposite directions with a total kinetic energy of approximately 160 MeV, creating extended defects in HTS in the form of two fission tracks. Fission tracks are made up of amorphous material and are approximately 10 μm long and 10 nm in diameter in Bi-based HTS superconductors [21]. The track structure is discontinuous and randomly oriented. U/n achieves its greatest success with highly anisotropic Bi-based (BSCCO) superconductors such as Bi-2223/Ag tape, where a 500-fold improvement in J_c was reported [22] at 77K and 0.8T for H//c. J_c for H//ab under the same conditions was nearly four orders of magnitude larger than for H//c before irradiation. There was also improvement after irradiation for H//ab, but J_c improved less than one order of magnitude. The anisotropy $J_c(H//ab)/J_c(H//c)$ was reduced 23 times at 0.5T and 77K. A 20-fold improvement in J_c at 77K and 0.25 T has been reported [23] in bulk melt textured $YBa_2Cu_3O_{7-\delta}$ (YBCO).

The discrepancy between the results for the YBCO and the Bi-2223 tape is due to the lesser anisotropy of YBCO. The vortices in HTS are two dimensional (2D) pancake vortices, residing on the CuO_2 planes [24, 25]. In highly anisotropic HTS, these pancake vortices in each CuO_2 layer can move independently from the vortices in the other CuO_2 layers. This makes it difficult to introduce effective pinning centres into such types of HTS, because vortices in each of the layers would have to be pinned down, giving an unacceptably high density of defects. However, if the pinning centres are in the shape of long columns traversing the CuO_2 planes, the pancake vortices in different layers will be collectively pinned along these columns and will thus be effectively aligned into vortex lines. Such pinning has been shown to be much more effective than pinning by point-like pinning centres [5].

The U/n method would seem to also be appropriate for MgB_2 . The reported coherence length values [3] of $\xi_{ab}(0) = 3.7-12$ nm and $\xi_c(0) = 1.6-3.6$ nm are of the same order as the expected diameter of the fission tracks introduced by high energy fragments resulting from the fission of ^{235}U . While it has been generally accepted that the optimal size of a pinning centre is twice the coherence length, there is also a theoretical indication that larger sizes up to the penetration depth λ may be effective under some circumstances [26]. Pinning centres of the size of λ would be effective if the pinning were dominated by electromagnetic interaction of vortices with pinning centres [27,28].

The U/n method would not be expected to produce anything like a 500-fold improvement in J_c in MgB_2 because the material is far less anisotropic than BSCCO. Reported results for the anisotropy coefficient $\gamma = \xi_{ab}/\xi_c$ range from 1.1 to 2.7 for textured bulk, aligned crystallites, films and single

crystals [3, 29]. By comparison, γ has been reported as 30 for Bi-2223/Ag tape [30] and 3 for melt-textured bulk YBCO [31]. There is no evidence of a 2D vortex state in MgB₂ bulk material, and the I-V characteristics have been reported as consistent with a vortex glass model [32, 33].

The most serious problem for the U/n method in MgB₂ is the enormous cross section of 3837 barn (b, where 1b = 10⁻²⁸ m²) for the ¹⁰B(n,α)⁷Li nuclear reaction. Here a ¹⁰B nucleus and a thermal (of the order of 25 meV) neutron react to form an α particle of kinetic energy 1.47 MeV and a ⁷Li nucleus with a kinetic energy of 0.84 MeV. By comparison, the ²³⁵U fission cross section is 584 b. Natural boron is comprised of 19.9% ¹⁰B, with the balance ¹¹B. The ¹⁰B(n,α)⁷Li reaction was deliberately used by Babic et al. [17] in an attempt to improve flux pinning by introducing ion tracks into MgB₂. An enhancement in the upper critical field was observed. However, the distribution of defects would have been extremely inhomogeneous because the thermal neutrons in this material have a mean free path of ~ 0.2 mm and thus only penetrated into a thin surface layer before being completely absorbed. The penetration depth increases with higher neutron energy, as the cross section for the ¹⁰B(n,α)⁷Li reaction decreases. At a neutron energy of 14 MeV the reaction cross section is 48.95 mb. Fast neutrons can create defects directly via elastic and inelastic scattering with the atomic lattice. However, defects produced by these mechanisms are considerably less significant than those produced via the ¹⁰B(n,α)⁷Li reaction when a full spectrum of neutron energies is employed [18]. In using the U/n method, it should be possible to significantly eliminate the competition for thermal neutrons between ¹⁰B and ²³⁵U by using highly enriched ¹¹B instead of natural boron. ¹¹B has a total thermal neutron cross-section of 5.05 b, almost all of it representing elastic scattering.

II. EXPERIMENTAL

To test the applicability of the U/n technique for enhancing J_c in MgB₂ an experimental program was designed. Powders of 1-11μm Mg from Hypertech (for samples A-D) or 325 mesh Mg (for sample E) and crystalline B (99.5 at% ¹¹B, particle size <22 μm, from Eagle-Picher) were mixed in a mortar in a stoichiometric atomic ratio of 1:2. Half of the powders were mixed with UO₂ (93% enriched in ²³⁵U) to give 1 wt% U. Optical microscopy revealed that the UO₂ particles ranged from 2-4 μm in diameter.

The powders were pressed into 0.4 g pellets, and the pellets sealed in iron tubes. Sintering took place in a tube furnace under flowing argon. For samples A-D the temperature was ramped up to 760° C over one hour. The pellets were held at that temperature for 30 min and then furnace cooled. For sample E the temperature was ramped up to 900° C over 1.5 h, and the pellets were held at that temperature for 3 h, then furnace cooled. The densities of the samples were 1.4 g/cm³ (samples A-D) and 1.0-1.1 g/cm³ (sample E). X-ray diffraction (XRD) was used to determine the phase composition of the doped and un-doped samples, while Energy Dispersive Spectroscopy (EDS) was used to determine the uranium distribution of doped samples. Portions of the doped and un-doped samples were then cut and filed into small regular rectangular blocks with dimensions of typically 3-4 × 3 × 2 mm³. The magnetisation and ac susceptibility were determined using a Quantum Design Physical Properties Measurement System (PPMS) in a time varying magnetic field with sweep rate 50 Oe/s and amplitude up to 8.5 T, with the applied magnetic field parallel to the longest dimension of the sample. The low field Zero Field Cooled (ZFC) and Field Cooled (FC) measurements were made with a Quantum Design Magnetic Properties Measurement System (MPMS). The J_c values at different magnetic fields and temperatures were calculated from the magnetic hysteresis loops using the Bean model: $J_c = 20\Delta M/[a(1-a/3b)]$, where a and b are the dimension of the sample perpendicular to the applied field, $a < b$. T_c was determined from the ac susceptibility measurements.

Small block samples, in doped and un-doped pairs, were double encapsulated in titanium capsules and irradiated by neutrons in HIFAR, a 10 MW DIDO class research reactor operated by ANSTO at

Lucas Heights, Australia. The irradiation rig was located within the graphite region of the reactor, and thus the neutron energy spectrum was highly thermalised with only a minimal fast and epithermal neutron component. The rig was rated with a nominal neutron flux of $\sim 1 \times 10^{13} \text{ n}\cdot\text{cm}^{-2}\cdot\text{s}^{-1}$. Four different fluences were used: $2 \times 10^{16} \text{ cm}^{-2}$ (A), $5 \times 10^{15} \text{ cm}^{-2}$ (B, E), $5 \times 10^{14} \text{ cm}^{-2}$ (C), and $5 \times 10^{13} \text{ cm}^{-2}$ (D). Following irradiation, the J_c and flux pinning properties of the irradiated pellets were then compared with the pre-irradiated results. The doped, irradiated samples were examined by transmission electron microscopy (TEM) to detect any fission tracks, and the extent of fission determined by gamma ray spectroscopy.

III. RESULTS AND DISCUSSION

X-ray diffraction (XRD) using a Philips 1730 phase XRD diffractometer showed that greater phase purity could be obtained using the longer, hotter sintering to fully react the crystalline boron and the magnesium (see Fig. 1). After 3 h at 900 C, the sintered un-doped sample E material (a) is MgB_2 with traces of Mg and MgO . The sintered 1wt% U-doped sample E material (b) also consists of MgB_2 with traces of Mg, MgO and UO_2 . Fig. 1(c) shows the un-doped sintered material characteristic of samples A-D. Because the sintering was shorter and at lower temperature the Mg and MgO impurity contents are much higher, due to the much larger amount of remaining un-reacted crystalline boron. These short sintering conditions are appropriate when amorphous boron is used to make MgB_2 . The impurities would be expected to give a smaller superconducting volume, but the intra-granular properties affected by the U/n method would not be degraded. For this reason samples from this lower quality material could also be used to determine the optimum neutron fluence.

Samples were characterised using a JEOL JXA-840 scanning electron microscope (SEM) equipped with a Link Systems AN10000 energy dispersive spectrometers (EDS). The results showed MgB_2 grains in a porous structure. The UO_2 particles remained separate, and the larger agglomerates could be distinguished at the grain boundaries. EDS analysis revealed the presence of large amounts of Mg and small amounts of U and Fe, the source of which was most likely the iron tubing containing the samples during sintering. The boron could not be detected with the experimental set-up. Figure 2(a) shows an EDS spectrum of the doped version of sample E. EDS mapping revealed a reasonably even distribution of UO_2 particles among the MgB_2 grains. Figure 2(b) shows the fairly even distribution of small UO_2 particles throughout the MgB_2 in sample E.

The ac susceptibility of the samples was measured at temperatures from 5 to 45 K and the magnetisation from 5 to 30 K using a Physical Properties Measurement System (Quantum Design, San Diego). T_c was determined from the ac susceptibility, and was not found to be significantly affected by irradiation and doping. T_c was measured to be 38.5 K with a sharp transition for the higher quality sample E regardless of doping and approximately 37.2 K for the other samples. The discrepancy is probably because samples A-D have a greater concentration of non-magnetic impurities, which are known to depress T_c in MgB_2 [34]. Figure 3(a) shows the derived values of the critical current at 5, 20 and 30K as a function of magnetic field for three versions of sample A ((i) un-doped and un-irradiated, (ii) doped with 1 wt% U, but not irradiated, and (iii) the same piece of doped sample A after irradiation with thermal neutrons at $2 \times 10^{16} \text{ cm}^{-2}$) and for sample B (doped with 1% U, then irradiated with thermal neutrons at $5 \times 10^{15} \text{ cm}^{-2}$). J_c values for sample E were similar, with a slightly lower H_{irr} , probably because the lower density cancelled out any benefits due to the higher purity. It is impossible to accurately determine J_c at 5K for very low fields because of the presence of thermal flux jumping [35]. J_c performance is slightly worse in the doped samples except at high magnetic fields, probably due to the presence of the additional impurities, but there are no significant differences between the irradiated and un-irradiated samples, in contrast to what has been demonstrated for HTS superconductors. The slightly worse performance of the high fluence irradiated sample A at high fields may be due to additional radiation damage from the higher neutron fluence. The discrepancy between the magnetisation for ZFC and FC

magnetisation measurements under superconducting conditions provides a measure of the pinning. Fig. 3(b) shows the ZFC-FC results at 100 Oe as a function of temperature for the doped, irradiated versions of samples A-D. There are no significant differences with fluence. Fig. 3(c) shows the pre-irradiation ZFC-FC results for the doped and un-doped versions of sample E. The higher T_c is attributed to the greater phase purity.

Transmission electron microscopy (TEM) was performed on two specimens (A and B) doped to 1 wt% U and irradiated to neutron fluences of $2 \times 10^{16} \text{ cm}^{-2}$ and $5 \times 10^{15} \text{ cm}^{-2}$ respectively. For both materials the microstructure was similar, that is, there were grains of MgB_2 several microns in diameter in which a number of dislocations and other crystalline defects were evident, but no fission tracks. Many such grains were examined, and Fig. 4(a) shows a typical example. This observation is in contrast to TEM studies of U-doped Bi-based HTS specimens exposed to similar levels of irradiation, in which the fission tracks appear as straight, randomly-oriented black lines due to the greater electron scattering from the amorphous material they contain. These fission tracks are several microns in length and clearly visible in TEM even at modest magnifications. This is illustrated in Figure 4(b), which shows a TEM image of the core of an irradiated, uranium-doped Bi-2223/Ag tape. A quantitative analysis of ^{235}U fissions in the present MgB_2 samples was obtained from the fission product yield as measured by the gamma-ray spectrometric method [36]. Measurements were limited to the doped, irradiated versions of samples C and D. A period of 92 days had expired since irradiation, which meant that most of the short-lived radioisotopes had decayed. This simplified the spectrum. To facilitate measurements, samples were placed 10 cm from the face of a large volume coaxial high purity germanium (HPGe) detector.

The gamma ray spectrum for sample C is shown in Figure 5. The spectral features were consistent with a 96 day decayed ^{235}U fission product spectrum [37]. The actual fission yield (see Table 1) was determined from the measured ^{137}Cs activity and the cumulative fission yield data for ^{137}Cs from ^{235}U . The cumulative yield includes the total number of ^{137}Cs atoms produced directly as a result of fission in addition to ^{137}Cs atoms produced via radioactive decay of the ^{137}Cs precursors, namely ^{137}I and ^{137}Xe which both have half-lives of less than 5 minutes. By comparison the half-life of ^{137}Cs is 30.17 years. The ^{137}Cs activity was determined from the peak area of the 662 keV emission and the known detector efficiency at this energy.

The fission yield can also be estimated from knowledge of the sample ^{235}U content, the cross section for fission of ^{235}U and the neutron fluence. The estimated fission yield along with the results from the gamma-ray spectrometric method is given in Table 1. A good correlation between estimated and measured fission yield was obtained. This shows that nuclear fission of ^{235}U did occur as expected. In HTS the same fission would produce columnar defects (Fig. 4(b)), resulting in strong pinning improvement. However, not a single fission track was observed for MgB_2 (Fig. 4(a)), and the field dependence of J_c was virtually unchanged after the irradiation (Fig. 3(a)).

An important parameter defining the creation of fission tracks is the electronic stopping power, also called the electronic energy loss, S_e [38]. It is defined as the energy transfer into the electronic excitations of the target atoms per unit length of the ion path through the target crystal. In our experiments, heavy ions of about 80 MeV are created by the nuclear fission and transfer their energy to the MgB_2 . The fission tracks can occur only if S_e exceeds a threshold value S_{e0} [39], which is dependent on the target material and the properties of the products of fission. The occurrence or otherwise of the fission tracks can be described by the thermal spike model [40, 41, 42]. In order to create fission tracks, there has to be a mechanism of energy transfer from the electrons to the crystal lattice. The thermal spike model does not explain the nature of these interactions, however, it explains the formation of the columnar defects in a thermodynamic approach. Because of the transfer of energy from the heavy ions to the electrons and subsequently to the crystal lattice on a longer time scale, a sudden localised increase in temperature occurs along the ion path through the crystal. For values of S_e higher than the threshold value S_{e0} , the crystal

lattice melts in a very localised volume along the ion track. Because the diameter of the molten volume is very small (of the order of a nanometre), this heat is diffused through the crystal lattice quickly enough to freeze the molten volume without allowing re-crystallisation. Consequently, a track of amorphous material is formed in the crystal, which is not superconducting and is expected to be a strong pinning centre.

In our experiments the fission tracks were clearly not formed. The reason for this may be that the S_e values were too low for the array of fission products interacting with MgB_2 , or that the heat conductivity required for freezing the molten volume is too low in MgB_2 , or that the energy transfer from the ions to the crystal electrons and the crystal lattice does not occur on timescales that would enable melting of the lattice. Because all of these factors are still unknown for MgB_2 , we cannot ascribe the observed lack of fission tracks to any of them in particular.

It is interesting to compare our results with experiments employing 2 MeV proton irradiation [14] as a means of improving the vortex pinning in MgB_2 . There, an improvement of the field dependence of J_c and the irreversibility field was observed. In HTS, protons of these energies were not capable of producing amorphous columnar defects, which are similar in nature to fission tracks [43]. To achieve such columnar defects, 800 MeV protons had to be used [44]. Therefore, the 2 MeV protons used in Ref. 14 were producing point defects in MgB_2 , which are much weaker pinning centres than columnar defects. However, due to the very large density of defects introduced, an observable increase of pinning was obtained. Point defects are also likely to be responsible for the improvement in pinning reported in Ref. 17 due to the $^{10}\text{B}(n,\alpha)^7\text{Li}$ nuclear reaction, rather than any ion tracks. Our results show a signature of point defects as well. There is a slight improvement of the field dependence of J_c at high fields for the highest neutron fluences (see Fig. 3(a)), accompanied by a slight decrease of J_{c0} and T_c . This may have occurred due to the point defects introduced by neutrons, as well as by the fission products. Because the neutron fluence employed here was much smaller than the proton fluence in Ref. 14, the improvement in the pinning was correspondingly smaller.

Confirmation of the nature of the crystallographic damage produced by both 2 MeV protons and ^{235}U fission particles in MgB_2 was obtained using particle transport simulation software [45]. Fission particles were simulated using ^{137}Cs ions with a kinetic energy of 60 MeV. Results revealed that the typical range of a 2 MeV proton in MgB_2 is about 45 μm . This can be compared to the typical range of a ^{137}Cs ion in MgB_2 of 10.6 μm . In terms of the number of Mg or B recoils produced, 2 MeV protons produced on average 25, as opposed to $\sim 33,000$ in the case of the ^{137}Cs ions. In terms of the damage structure, protons produced small damage regions consisting of isolated point defects localised about the end of the proton range. In comparison, the ^{137}Cs ions produced large damage clusters containing several hundred displaced atoms. The clusters were located along the track of the ions, although most damage was again located within the last 2-3 μm of the track. In both cases annealing of the displacement damage immediately following creation could be expected due to thermally assisted diffusion of atoms back to their correct crystallographic sites. The thermal energy assisting this process is sourced directly from the interacting primary and secondary particles produced in the actual displacement event. Longer term annealing may also be expected due to room temperature assisted processes. The fraction of annealing occurring within the fission particle damaged material is expected to be greater than that within the proton irradiated material. This is on account of the increased density of damage within the clusters of the fission particle damaged material as opposed to the more isolated point defects predicted in the proton-irradiated material. The damage remaining in the fission particle damaged material is still expected to be much greater than that found in the proton-irradiated material.

IV. SUMMARY

MgB₂ samples were made of highly enriched ¹¹B in a reaction in-situ process and doped with UO₂ containing highly enriched ²³⁵U to a doping level of 1 wt% U. The samples were then irradiated with thermal neutrons at fluences ranging from $5 \times 10^{13} \text{cm}^{-2}$ to $2 \times 10^{16} \text{cm}^{-2}$. The intent was that the ²³⁵U atoms would fission and that the fission fragments would create columnar amorphous damage tracks to act as pinning centres to trap magnetic flux and improve critical current performance in the MgB₂ superconductor. There was no evidence of such tracks in TEM. This is consistent with the lack of evidence of improved critical currents in magnetic fields as a result of the irradiation. Gamma-ray spectroscopy indicated that fission of the ²³⁵U atoms had taken place as expected and was not hindered by the presence of any residual ¹⁰B. The reason for the absence of the tracks is not yet clear, because the threshold electron stopping power and the mechanisms of the energy transfer to the crystal lattice are still not known for the interaction of ²³⁵U fission fragments with MgB₂.

ACKNOWLEDGEMENTS

We wish to thank X.L. Wang, K. Konstantinov, A. Pan, M.J. Qin, M. Ionescu, and B.R. Winton of the Institute for Superconducting and Electronic Materials and D. Wexler of the Faculty of Engineering, University of Wollongong for practical help and useful discussions. The authors would also like to thank the Australian Institute of Nuclear Science and Engineering for providing assistance (Award No. 02/121) to enable the work on MgB₂ to be conducted.

-
- ¹ J Akimitsu 2002 *Symposium on Transition Metal Oxides (Sendai, Japan, 10 January 2001)*.
- ² J. Nagamatsu, J. Nakagawa, T. Muranaka, Y. Zenitani and J. Akimitsu, *Nature* **410** (2001), 63.
- ³ C. Buzea and T. Yamashita, *Supercond. Sci. Technol.* **14** (2001) R115.
- ⁴ C.B. Eom, M.K. Lee, J.H. Choi, L.J. Belenky, X. Song, L.D. Cooley, M.T. Naus, S. Patnaik, J. Jiang, M. Rikel, A. Polyanskii, A. Gurevich, X.Y. Cai, S.D. Bu, S.E. Babcock, E.E. Hellstrom, D.C. Larbalestier, N. Rogado, K.A. Regan, M.A. Hayward, T. He, J.S. Slusky, K. Inamaru, M.K. Haas and R.J. Cava, *Nature*, 2001, **411**, 558.
- ⁵ M.E. McHenry and R.A. Sutton, *Progress in Materials Science* **38** (1994) 159.
- ⁶ K.H.P. Kim, W.N. Kang, M.S. Kim, C.U. Jung, H.J. Kim, E.M. Choi, M.S. Park and S.I. Lee, *Physica C* **370** (2002) 13.
- ⁷ Y. Bugoslavsky, G.K. Perkins, X. Qi, L.F. Cohen and A.D. Caplin, *Nature* **410** (2001) 563.
- ⁸ H.H. Wen, S.L. Li, Z.W. Zhao, H. Jin, Y.M. Ni, W.N. Kang, H.J. Kim, E.M. Choi and S.I. Lee, *Phys. Rev. B* **64** (2001) 134505.
- ⁹ H.H. Wen, S.L. Li, Z.W. Zhao, H. Jin, Y.M. Ni, Z.A. Ren, G.C. Che and Z.X. Zhao, *Physica C* **363** (2001) 170.
- ¹⁰ D.C. Larbalestier, L.D. Cooley, M.O. Rikel, A.A. Polyanskii, J. Jiang, S. Patnaik, X.Y. Cai, D.M. Feldmann, A. Gurevich, A.A. Squitieri, M.T. Naus, C.B. Eom, E.E. Hellstrom, R.J. Cava, K.A. Regan, N. Rogado, M.A. Hayward, T. He, J.S. Slusky, P. Khalifah, K. Inamaru and M. Haas, *Nature* **410** (2001) 186.
- ¹¹ D.S. Fisher, M.P.A. Fisher and D.A. Huse, *Phys.Rev.B* **43** (1991) 130.
- ¹² S.X. Dou, S. Soltanian, J. Horvat, X.L. Wang, S.H. Zhou, M. Ionescu and H.K. Liu, *Appl.Phys.Lett.* **81** (2002) 3419.
- ¹³ X.L. Wang, S.H. Zhou, M.J. Qin, P.R. Munroe, S. Soltanian, H.K. Liu and S.X. Dou, cond-mat/0208349, to be published in *Physica C*.
- ¹⁴ Y. Boguslavsky, L.F. Cohen, G.K. Perkins, M. Polichetti, T.J. Tate, R. Gwillam and A.D. Caplin, *Nature* **411** (2001) 561.
- ¹⁵ H. Narayan S.B. Samanta A. Gupta, A. V. Narlikar, R. Kishore K.N. Sood, D. Kanjilal, T. Muranaka and J. Akimitsu, *Physica C*. **377** (2002) 1.
- ¹⁶ R.J. Olsson, W.-K. Kwok, G. Karapetrov, M. Iavarone, H. Claus, C. Peterson and G.W. Crabtree, cond-mat/0201022.
- ¹⁷ E. Babic, B. Miljanic, K. Zadro, I. Kusevic, Z. Marohnic, D. Drobac, X.L. Wang and S.X. Dou, *Fizika A* **10** (2001) 87.
- ¹⁸ M. Eisterer, M. Zehetmayer, S. Tonies and H.W. Weber, *Supercond. Sci. Technol.* **15** (2002) L9.
- ¹⁹ R. Weinstein, Y. Ren, J. Liu, I. Chen, R. Sawh, C. Foster and C. Obot, *Proc. Int. Symp. on Superconductivity, Hiroshima, 1993*. (Springer, Berlin, 1993) p. 285.
- ²⁰ G.W. Schulz, C. Klein, H.W. Weber, S. Moss, R. Zeng, S.X. Dou, R. Sawh, Y. Ren and R. Weinstein, *Appl.Phys.Lett.* **73** (1998) 3935.
- ²¹ S. Tönies, H.W. Weber, Y.C. Guo, S.X. Dou, R. Sawh and R. Weinstein, *Appl. Phys. Lett.* **78** (2001) 3851.
- ²² S.X. Dou, Y.C. Guo, D. Marinaro, J.W. Boldeman, J. Horvat, P. Yao, R. Weinstein, A. Gandini, R. Sawh and Y. Ren, *IEEE Trans.Appl.Supercond.* **11** (2001) 3896.
- ²³ M. Eisterer, S. Tonies, H.W. Weber, R. Weinstein, R. Sawh and Y. Ren, *Physica C* **341-348** (2000) 1439.
- ²⁴ J. R. Clem, *Phys. Rev. B*. **43** (1991) 7837.

-
- ²⁵ J.R. Clem, *Physica C* **162-164** (1989) 1137.
- ²⁶ N. Takezawa and K. Fukushima, *Physica C* **290** (1997) 31.
- ²⁷ G.S. Mkrchyan and V.V. Shmidt, *Sov. Phys. JETP* **34** (1972) 195.
- ²⁸ W.E. Timms and D.G. Walmsley, *Phys. Stat. Solidi B* **71** (1975) 741.
- ²⁹ A. Dulcic, M. Pozek, D. Paar, E.M. Choi, H.J. Kim, W.N. Kang and S.I. Lee, cond-mat/0207655.
- ³⁰ J.P. Fagnard, P. Vanderbemden, D. Crate, V. Misson, M. Ausloos and R. Cloots, *Physica C* **372** (2002) 970.
- ³¹ P. Vanderbemden, R. Cloots, M. Ausloos, R.A. Doyle, A.D. Bradley, W. Lo, D.A. Cardwell and A.M. Campbell, *IEEE Trans. Appl. Supercond.* **9** (1999) 2308.
- ³² M.B. Maple, B.J. Taylor, N.A. Frederick, S. Li, V.F. Nesterenko, S.S. Indrakanti and M.P. Maley, *Physica C* **382** (2002) 132.
- ³³ G.K. Gupta, S. Sen, A. Singh, D.K. Aswal, J.V. Yakhmi, E.M. Choi, H.J. Kim, K.H.P. Kim, S. Choi, H.S. Lee, W.N. Kang and S.I. Lee, *Phys. Rev. B* **6610** (2002) 4525.
- ³⁴ E. Cappelluti, C. Grimaldi and L. Pietronero, cond-mat/0211481.
- ³⁵ S.X. Dou, X.L. Wang, J. Horvat, D. Milliken, A.H. Li, K. Konstantinov, E.W. Collings, M.D. Sumption and H.K. Liu, *Physica C* **361** (2001) 79.
- ³⁶ IAEA, "Compilation and evaluation of fission yield nuclear data", IAEA-TECDOC-1168 (2000).
- ³⁷ R.L. Heath, "Gamma-ray spectrum catalog", ANCR-1000-2.
- ³⁸ Y. Zhu, Z.X. Cai, R.C. Budhani, M. Suenaga and D.O. Welch, *Phys. Rev. B* **48** (1993) 6436.
- ³⁹ J. Provost, Ch. Simon, M. Hervieu, D. Groult, V. Hardy, F. Studer and M. Toulemonde, *Materials Research Society Bulletin* **20** (1995) 22.
- ⁴⁰ G. Szenes, *Phys. Rev. B* **51** (1995) 8026.
- ⁴¹ F. Seitz and J.F. Koehler, in *Solid State Physics: Advances in Research and Applications*, edited by F. Seitz and D. Turnbull, Academic, New York, 1995, vol. 2, p. 305.
- ⁴² M. Toulemonde, C. Dufour and E. Paumier, *Phys. Rev. B* **46** (1992) 14362.
- ⁴³ L. Civale, A.D. Marwick, M.W. McElfresh, T.K. Worthington, F.H. Holtzberg, J.R. Thompson and M.A. Kirk, *Phys. Rev. Lett.* **65** (1990) 1164.
- ⁴⁴ H. Safar, J.H. Cho, S. Fleshler, M.P. Maley, J.O. Willis, J.Y. Coutler, J.L. Ullman, P.W. Liowski, G.N. Riley, M.W. Rupich, J.R. Thompson and L. Krusin-Elbaum, *Appl. Phys. Lett.* **67** (1995) 130.
- ⁴⁵ J.F. Ziegler and J.P. Biersack, *The Stopping and Range of Ions in Solids*, Pergamon Press, New York, 1985.

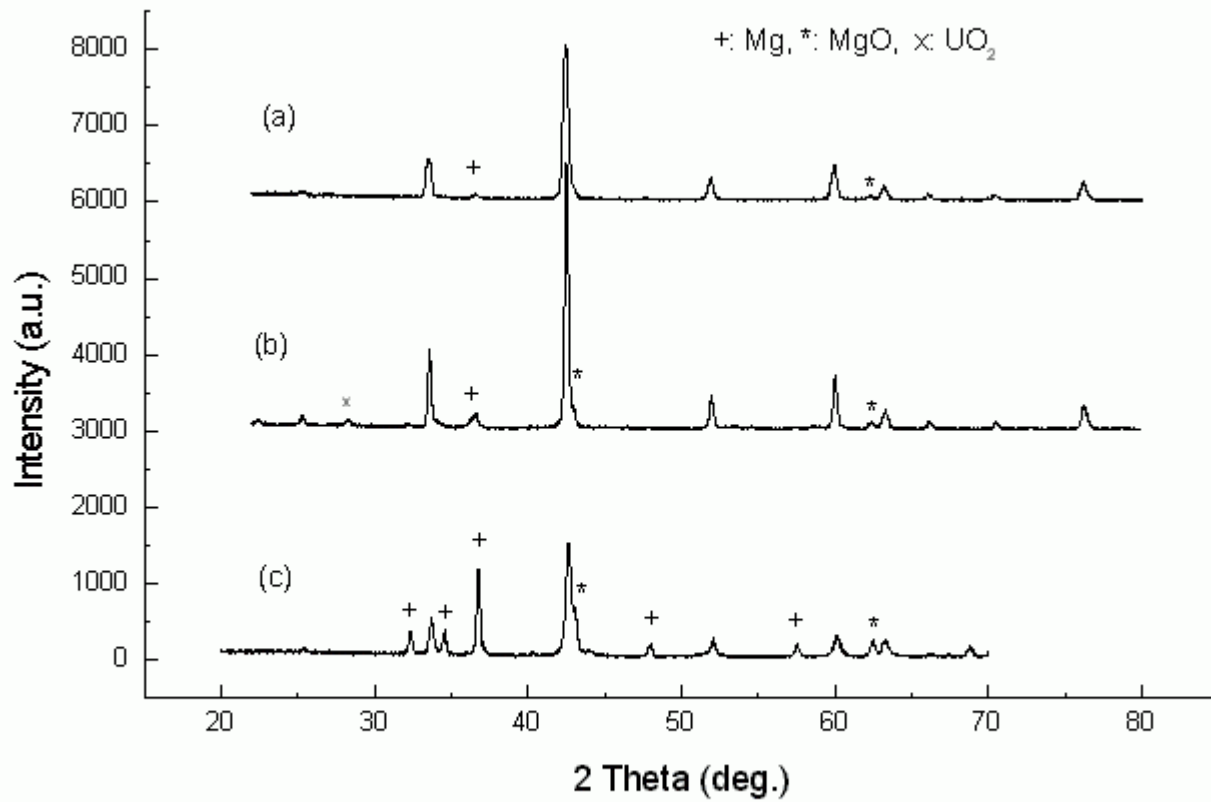
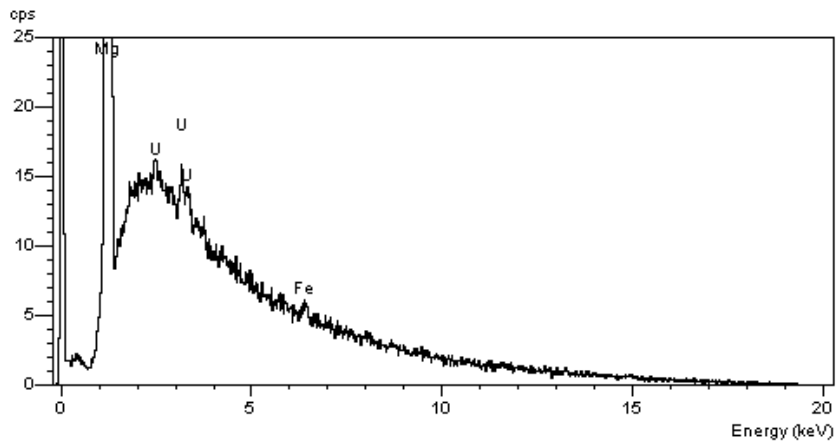
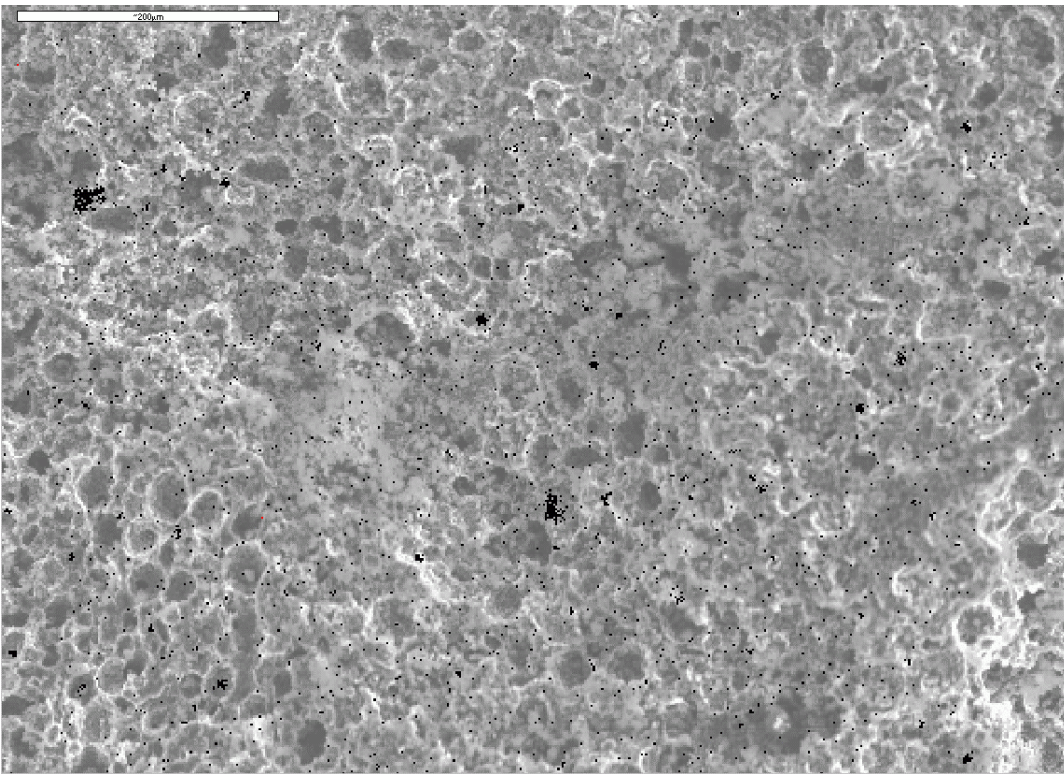


Fig. 1

Figure 1. XRD spectra of the MgB₂ used for the samples. (a) undoped, sintered at 900 C for 3h; (b) doped with 1 wt% U as UO₂, sintered at 900 C for 3 h; (c) undoped, sintered at 760 C for 0.5 h. The MgB₂ phase peaks are unmarked.



a)



b)

Figure 2. (a) Averaged EDS spectrum of sample E doped with 1 wt % uranium; (b) EDS mapping of a cross-sectional area of sample E showing the distribution of the UO₂ particles in black.

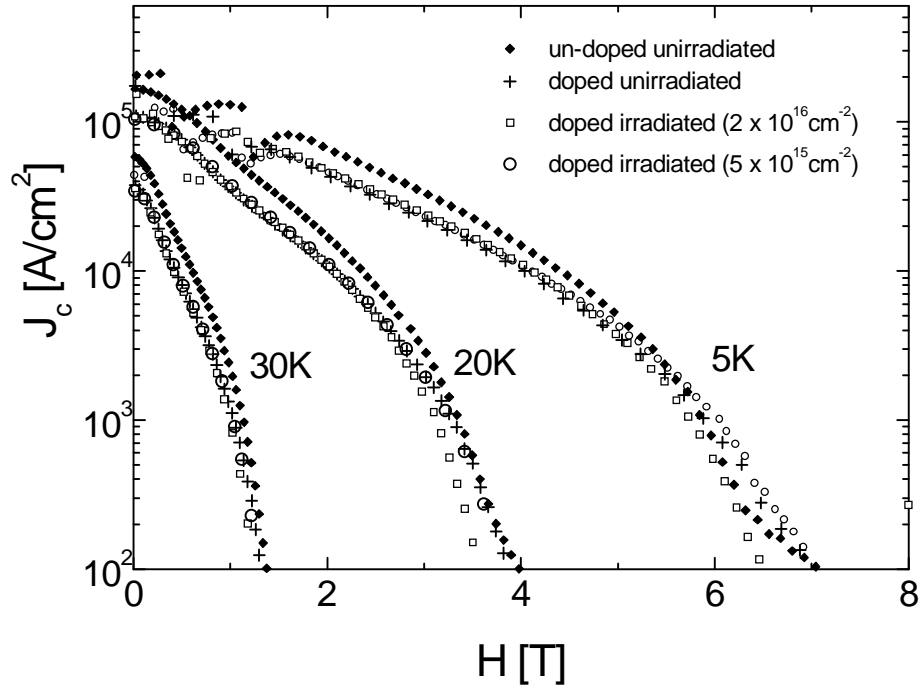


Fig 3 a)

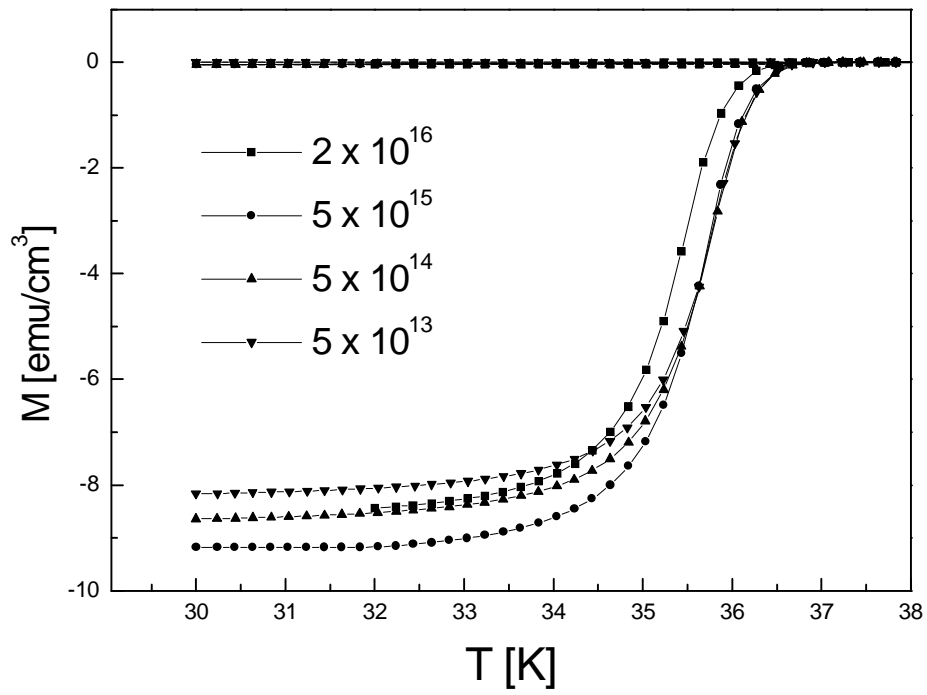


Fig 3b)

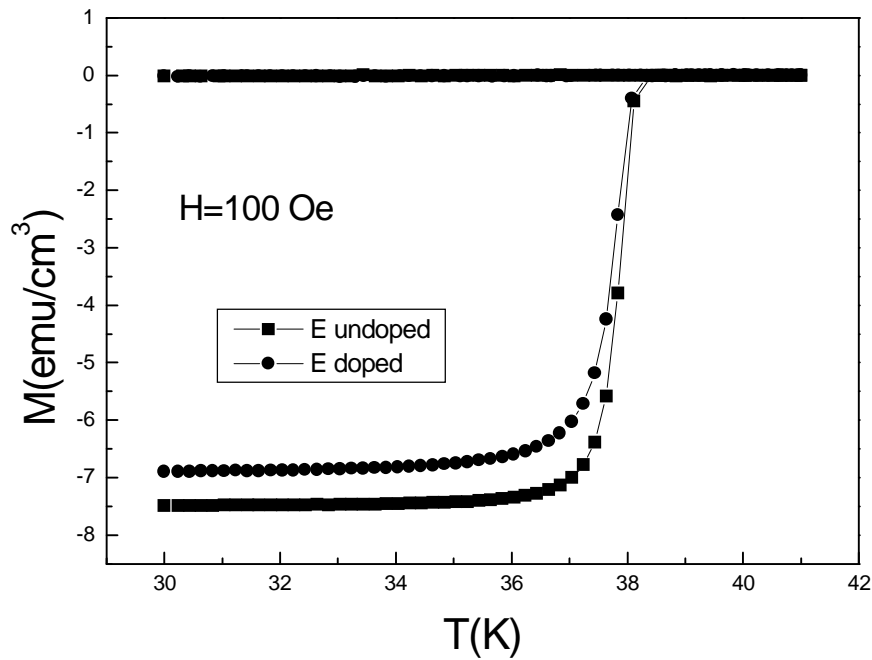


Fig. 3(c)

Figure 3. (a) Critical current derived from PPMS measurements as a function of magnetic field at 5, 20 and 30K for sample A (un-doped and doped with 1 wt% U). J_c for the doped version of sample A is shown before and after irradiation at $2 \times 10^{16} \text{ cm}^{-2}$ with thermal neutrons. J_c for the doped version of sample B (also 1 wt% U) is shown after irradiation with thermal neutrons at $5 \times 10^{15} / \text{cm}^2$. (b) The magnetisation under ZFC and FC conditions as a function of temperature at a field of 100 Oe as determined by MPMS measurements. All the samples shown were doped to 1 wt% U and irradiated at the fluences $/\text{cm}^2$ that are shown in the legend. (c) MPMS measurements under the same conditions for the un-irradiated high purity sample E, both un-doped and doped to 1 wt% U.

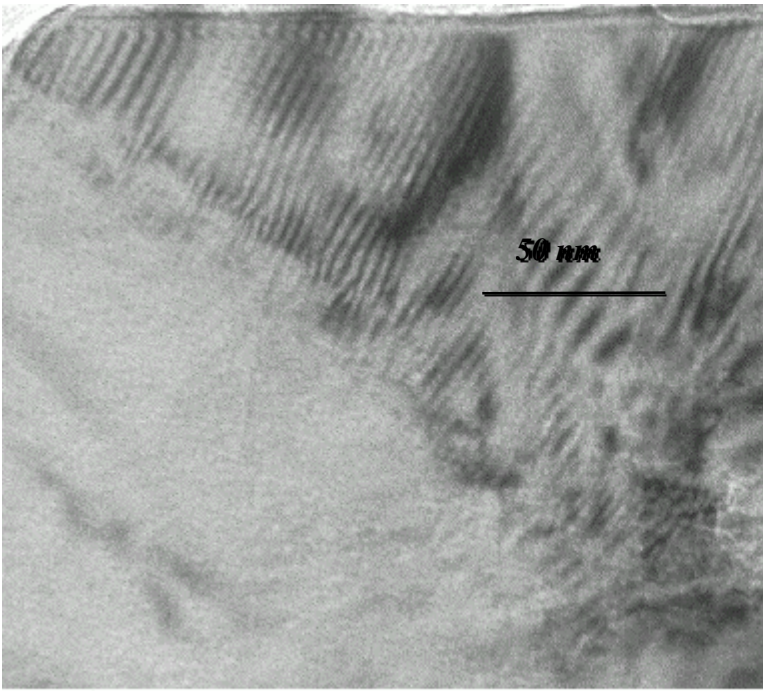


Fig. 4(a)

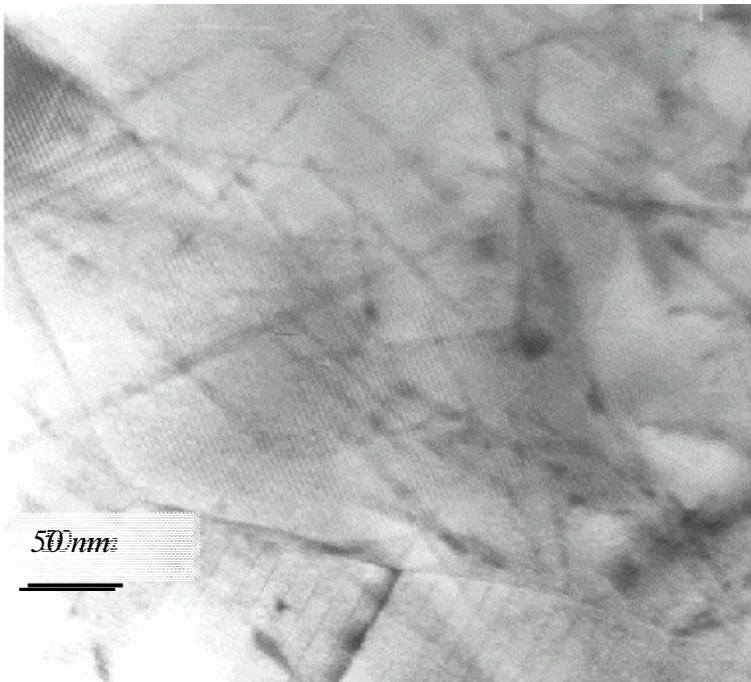


Fig. 4(b)

Figure 4. (a) Typical TEM image of an MgB₂ grain from sample B (doped to 1 wt% U and irradiated at $5 \times 10^{15} \text{ cm}^{-2}$ with thermal neutrons). This grain, like all the others examined, shows no evidence of columnar defects that might be due to fission tracks. (b) TEM image of the core of a U-doped irradiated Bi-2223/Ag tape showing fission tracks.

Table 1: Comparison of ^{235}U fission yield estimated prior to irradiation and measured after irradiation using the gamma-ray spectrometric technique.

Sample	^{235}U fission yield (Calculated)	^{235}U fission yield (Gamma spectrometric method)
C	1.93×10^{11}	1.06×10^{11}
D	2.31×10^{10}	3.04×10^{10}